Some Mechanisms of Oceanic Mixing Revealed in Aerial Photographs[1]

G. ASSAF, R. GERARD AND A. L. GORDON

Lamont-Doherty Geological Observatory, Columbia University, Palisades, New York 10964

Estimates of circulation rates within the mixed layer of the ocean have been made based on aerial photographs of a variety of dye injections and floating cards in the surface and near-surface levels under different wind, sea state, and thermal profile conditions. The following are the main features derived from our studies of the circulation patterns in the mixing layer in the Bermuda area. (1) Except under calm conditions, the first few meters of the sea are subjected to helical flow of small-size Langmuir cells with 3 to 6 meter spacing between the convergence lines. (2) Under moderate to strong wind conditions (10–30 knots), a hierarchy of larger-size Langmuir cells is developed. The maximum horizontal spacing between the larger cells is approximately the same as the depth of the mixing layer. The spacing of the convergence zones between the largest cells was 280 meters, and they were accompanied by medium and small-size cells of approximately 35 and 5 meters, respectively. Estimates of the apparent vertical diffusion associated with the large and medium Langmuir cells are thousands and hundreds of cm^2/sec, respectively. (3) A stratified flow resembling an Ekman spiral is observed under moderate conditions. (4) There is coexistence between the small-size Langmuir cells and the Ekman spiral below. However, when the large Langmuir cells are developed, the flow pattern in the mixing layer does not resemble an Ekman spiral. The transition from the Ekman to the Langmuir regime occurs with turbulence Reynolds numbers of approximately 100. (5) Under calm conditions following a period of moderate winds and thermal instability, we observed convergence zones having anticyclonic rotation with inertial period.

The general statistical approach: Achievement and limitation. The study of oceanic mixing has, for the most part, been dominated by the statistical approach. The main achievement of this approach has been the establishment of the relationship between the dispersion rate and the scale of diffusion.

It is well recognized that the mixing process in the sea is characterized by Richardsonian, rather than Fickian, diffusion [*Stommel*, 1949]. This means that the diffusion rate of a given cloud of soluble matter in the sea depends on interaction with eddies of size and age similar to the cloud. One of the main consequences of this is that a single cloud cannot recognize the stochastic nature of these eddies because of 'bad' or insufficient statistics. To be more statistically meaningful, clouds of different sizes should be grouped in different ensembles and the diffusivity of any cloud should then be related to the diffusivity of ensemble means of clouds of similar size and age. Such an attempt was made by *Okubo* [1971] when he summarized twenty sets of dye experiments of different scales by introducing them into a diffusion diagram. By reference to this diagram (Figure 1), one can obtain the mean statistical features of oceanic diffusion for different time scales and sizes. However, this diagram cannot give detailed predictions, since the expected variation in the diffusion rate under different experimental conditions is more than an order of magnitude.

The hazards of the statistical approach are exemplified in our experiment on January 29, 1970. This experiment was designed to explore the statistical approach by deploying many dye patches over a large area to examine the effects of different diffusion scales. The surprising result was that the whole dye field shrank, indicating that the horizontal eddy diffusion of the field enclosed by the dye patches was actually negative in the observed scales. Probably such unpredictable behavior made *Okubo* [1970] close his review on oceanic mixing with the statement 'diffusion is confusion.'

The January experiment and others have

[1] Contribution 1695, Lamont-Doherty Geological Observatory.

forced us to ignore, for the time being, the statistical method and to concentrate on studies of the actual mechanisms which cause differential motion between clouds of dye or within one dye body.

EXPERIMENTAL PROCEDURES

The serial observations and measurements in the Bermuda area were carried-out from a four-engine C-121 aircraft operated by the U. S. Naval Oceanographic Office. The following instrumentation and methods (summarized in Figure 2) were used:

Air-drop dye buoys. These devices, constructed from surplus Navy sonobuoy cases, are ejected pneumatically from the aircraft's sonobuoy launching tubes at a minimum altitude of 500 feet and at an air speed of about 160 knots. The dye buoy dropped to the sea surface in an upright attitude, stabilized by its four-bladed rotochute. Upon impact, the weighted bottom plate separated from the buoy and fell to the sea bottom to become the anchor, carrying with it a nylon filament anchor line. The buoys are capable of anchoring in depths as great as 200 meters.

Alternating red (rhodamine) and yellow (fluorescein) dye cakes (approximately 100 grams each) were attached to the anchor line at depths of 1, 4, 7, and 10 meters below the surface buoy. These dye sources generated colored plumes at their respective depths for about one hour, during which time the dye pattern was photographed from the aircraft on successive passes. The maximum depth of visibility of the dye in the Bermuda area was generally greater than 10 meters.

Surface current marker. As the rotochute fell away on dye buoy impact, a free-floating dye cake was deployed to serve as a surface current marker. This unit, which is designed to have a minimum of windage, drifted and created a dye mark in the top few centimeters of water. Its progressive separation from the anchored buoy, recorded on aerial photographs, revealed surface current speed and direction.

Smoke generators. A sea-surface chemical smoke marker was normally dropped at the same location as a dye buoy, so that both dye and smoke plumes would appear in the same photographic field. Distances from the smoke source to identifiable features of the smoke plume were measured on sequential photographs taken at known intervals (usually 4 sec) to reveal wind speed. The relative direction of the smoke plume's main axis was compared to the known aircraft heading to obtain wind direction. Wind speeds measured from the aerial photographs agreed within 10% with conventional wind measurements taken at the Argus Island Tower on Plantagenet Bank near Bermuda.

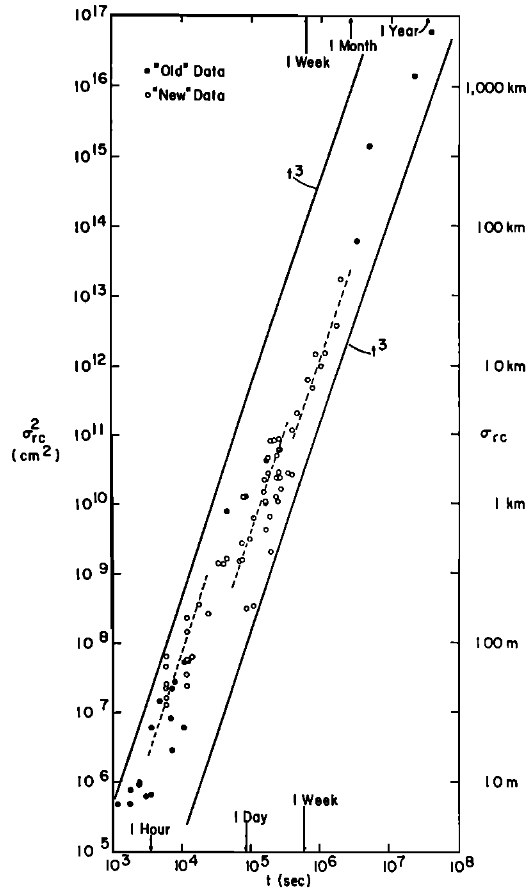

Fig. 1. The empirical relations between the variance of the concentration of soluble tracer (mostly dye) in the sea surface and time [from *Okubo*, 1971].

Multiple deep-station dye plumes. Dye plumes were generated at the deep (3000 meter) station south of Bermuda using a taut-wire anchored buoy (deployed by a ship), to which was tethered a small auxiliary buoy. Dye cakes were suspended below the auxiliary buoy in an array similar to that used in the air-drop buoys.

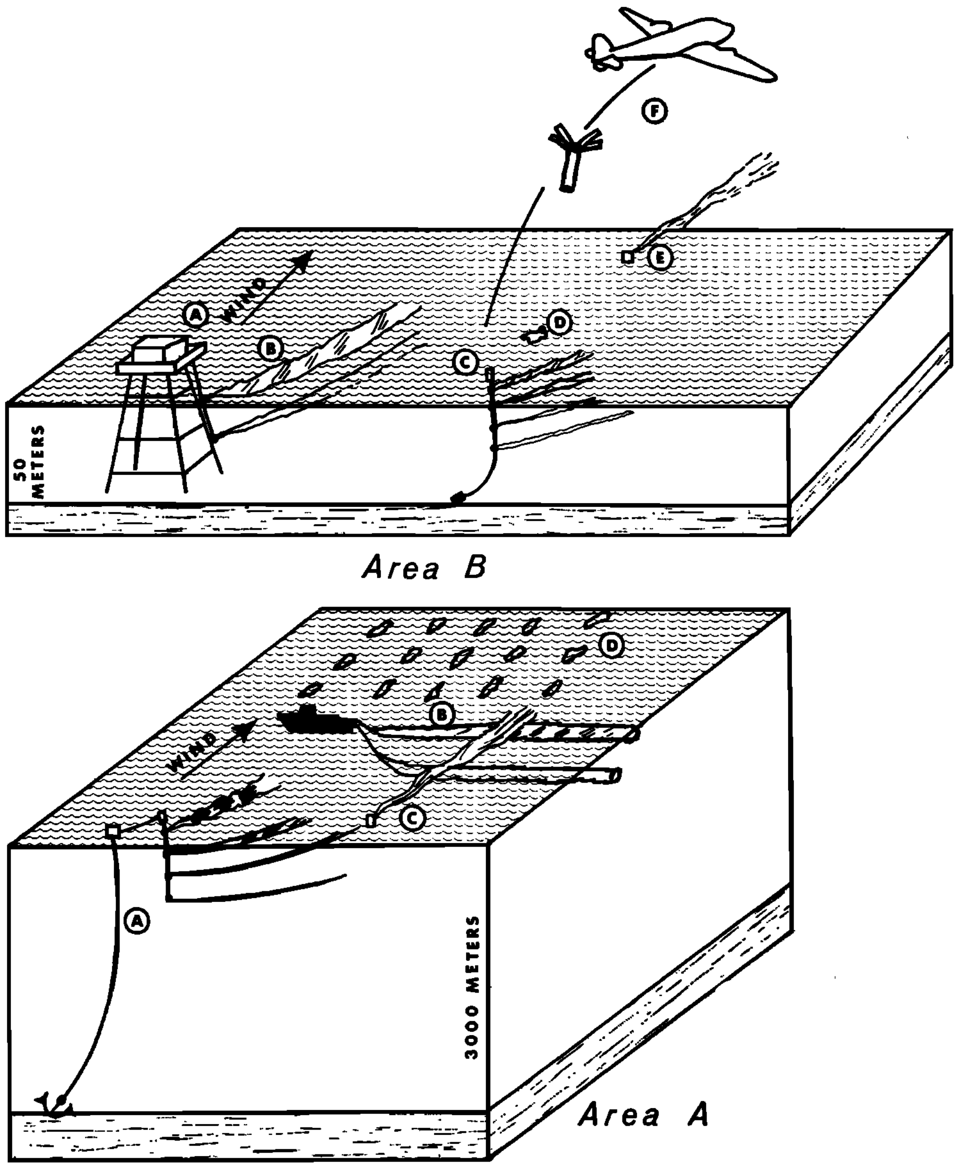

Fig. 2. Schematic diagram of the experimental procedures used in the Bermuda experiments.

Dye stripes and floating cards. At the deep (3000 meters) station south of Bermuda, the ship, moving at 3 knots, pumped liquid dye at a rate of 2 liters/min at two levels along a track perpendicular to the wind, creating superimposed dye stripes about 1 km in length. Red (rhodamine B) dye was pumped at the surface, and yellow-red (rhodamine 5GDN) dye was pumped at a 6-meter depth in this operation. After completing the dye run, the ship reversed course and disbursed paper cards (old IBM cards) along a track parallel to and windward of the dye stripes. The cards, floating at the surface, invariably broke up into long lines parallel to the wind and moved through the dye stripe. The patterns of dye and cards were photographed from the air in successive passes, which normally included photography over the nearby multiple deep-station dye plumes.

Metered dye plumes. Using the Argus

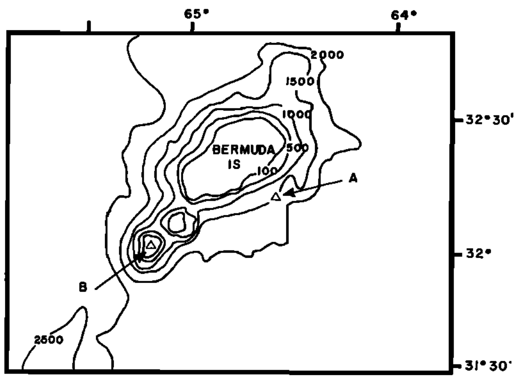

Fig. 3. Location map of experimental sites near Bermuda (depth given in fathoms).

Tower, located on the 50-meter deep Plantagenet Bank, liquid dye was pumped at two levels at the rate of 1 ml/sec while photographic overflights were made. Red (rhodamine B) dye was pumped at the surface and yellow-red (rhodamine 5GDN) dye at 6 meters during a 2- to 4-hour period. During this time large plumes up to 1-km in length commonly developed.

Dye bombs. One-gallon plastic containers of liquid rhodamine or fluorescein dye were deployed through the open door of the aircraft at an altitude of 2500 feet. Commonly, about five dye bombs were dropped along each of five parallel lines to create a 1-km^2 field of dye patches with approximately 200-meter spacing. The field was photographed from various altitudes up to 5000 feet at intervals during a 4- to 6-hour period.

Aerial photography. Vertical aerial photographs were taken using a standard CA-14 photogrammetric camera with Kodak Ektachrome aero film. Photographic runs were normally made at an altitude of 1500 feet at 160 knots with a 4-sec frame interval, providing an overlap of approximately 50% on the 9-inch film frames. The individual frames were automatically marked with altitude, time, and frame number for ease of data storage and interpretation.

A hand-held 35mm camera was also used from the aircraft observer's bubble on photographic runs to obtain oblique photos to supplement the data obtained with the automatic camera.

OBSERVATIONS

Experiment of March 19, 1970: Eddy viscosity (Ekman) versus Langmuir circulation. The Ekman spiral [*Ekman*, 1905] and Langmuir cells [*Langmuir*, 1938] are two concepts associated with wind-driven ocean currents. To some extent, the Ekman concept of eddy viscosity is not consistent with the transport mechanism associated with large, semi-organized cellular motion as discussed by *Langmuir* [1938]. The results of our March 19 experiment give insights into both processes.

In this experiment we attempted to compare the oceanic surface mixing at a deep ocean site and a nearby shallow site. The locations of this experiment are given in Figure 3. Area A is over the deep ocean (3000 meters) and B is over shallow water (50 meters). Weather conditions are given in Table 1. The wind changed from north to south on March 18 prior to our experiment. The wind speed was very small during the night of March 18–19 and increased on March 19. Thus the experiment was carried out under transient wind stress, from calm to moderate conditions. A temperature profile down to 300 meters was measured with an air-expendable bathythermograph (AXBT). This profile shows a uniform temperature down to 200 meters and a decrease in temperature of 1°C in the lower 100 meters.

To obtain a general idea of the circulation pattern over the deep water location (site A), 36 dye bombs were deployed from the aircraft in the manner already described. The distribution of the dye patches from these bombs at 1000 hours is given in Figure 4. The distribution of the dye field after an hour and a half is superimposed on the original distribution. The general impression is that the dye patches elongated along lines that were more or less in one direction. Besides the elongation of the dye patches themselves, it can be seen that the orientation of the whole dye field changed as it rotated clockwise. Interestingly enough, the change of orientation of the dye field between 1000 and 1127 hours is about 0.35 radians, which is equivalent to inertial rotation at that latitude ($T_i = 8 \times 10^4$ sec).

Because the aircraft was not available for an extended series of photographic runs, we cannot say much about the mechanism and the dynamics that controlled this mixing and elon-

TABLE 1. Weather Observations at Kindley, Bermuda

	Wind Direction	Wind Speed, knots	Temperature	Dew
January 28				
0200 LT	310°	15	17°C	11°C
0800 LT	340°	17	17°C	6°C
1400 LT	350°	14	16°C	5°C
2000 LT	010°	6	15°C	5°C
January 29				
0200 LT	calm	0	13°C	5°C
0800 LT	190°	3	17°C	8°C
1400 LT	190°	7	17°C	9°C
2000 LT	190°	15	17°C	11°C
March 18				
0200 LT	350°	2	13°C	4°C
0800 LT	350°	2	15°C	6°C
1400 LT	40°	5	17°C	8°C
2000 LT	110°	3	16°C	7°C
March 19				
0200 LT	130°	9	16°C	10°C
0800 LT	150°	11	17°C	12°C
1400 LT	170°	11	20°C	12°C

gation. However, a dye stripe, generated from our ship near the dye patches at a depth of 6 meters in a straight line perpendicular to the wind, revealed some of the detail of the mixing mechanism (Figure 5). Two scales of semi-organized cells were observed. The largest size

Fig. 4. The distribution of the dye patches on March 19, 1970 at 1127 hours superimposed on the distribution at 1000 hours.

is indicated by the curvature which developed between 0937 and 0958, when dye converged and accelerated in two cells 280 meters apart.

The evolution of the smaller cells can also be observed as they become distinct parcels of dye with spacing of approximately 40 meters in the later stages. Floating cards, deployed by the method already described, converged first along lines which coincided with the axes of the medium-size dye cells. At 0958 the cards appeared to concentrate along a line in the eastern side of the dye stripe, which coincided with the forward portion of a large dye cell. The convergence of the cards and the concentration of dye along the same axes strongly suggest that the formation of these axes of forward motion are accompanied by horizontal convergence of surface water.

The forward motion at the divergence zone is less than that found at the convergence (as noted by *Langmuir* [1938] and in the review article of *Scott et al.* [1969]). This shear (in the largest cells) results in the observed curvature of the dye stripe. The shear between the convergent and divergent zones, accompanied by vertical motion within these zones, is responsible for the downward flux of momentum [*Gordon,* 1970].

During both morning and afternoon experiments, anchored dye-plume generators were deployed and photographed together with the nearby dye stripes. The plume generators, which inject dye at four levels within the upper 10 meters, are designed to show the vertical structure of the near-surface current. When the current is uniform (i.e., the current is only a function of depth), the plumes which develop at the different depths show a regular pattern which follows the current structure (see, for example, Figure 10). However, the generated plumes at site A were very quickly mixed in one dye patch (Figure 6), and one could not distinguish the different depths. Langmuir cells of different sizes seemed to dominate the mixing, and no evidence of current stratification associated with the Ekman spiral was observed under these circumstances.

By comparing the sequential photographs of the different parts of the stripe, it is possible to estimate the shear between the convergent and divergent zones. Another method to determine shear is based on the elongation of the dye patches. Applying both methods, the forward velocity of the convergence is estimated to be 10 cm/sec.

The original photographs of the dye stripe in the morning (0958) are given in Figure 7. By comparing the velocity between the dye stripe and the nearby anchored buoy, it was determined that the whole dye stripe drifted in the direction of the wind at a velocity of 12 cm/sec.

Figure 8 presents a second time sequence of the stripe, generated in the same area in the afternoon. In this experiment, red dye was pumped at a depth of 1 meter and yellow dye at 6 meters. The results look essentially the same. We can recognize the larger sizes of Langmuir cells, 280 and 35 meters. In addition, the microstructure of the dye (Figure 9) clearly shows cells of 4 to 5-meter size. While the dye stripe drifted as a whole in the direction of the wind in the morning, in the afternoon it drifted to the right of the wind.

To what extent will shallow water modify the pattern of mixing? Air-drop dye buoys were deployed (see experimental procedures) on the same day over the flat, 50-meter-deep Plantagenet Bank. The bank is nearly circular, with a diameter of 9 km, and is surrounded by deep ocean. The multiple plumes that developed in both morning and afternoon experiments (Figure 10) resembled the typical Ekman spiral. Especially in the afternoon plumes 3 and 4 show a very regular velocity gradient with depth and deviation of the deeper plumes to the right. Using the Ekman model, the depth of the Ekman layer can be estimated from the angle between the plumes or from the velocity gradient.

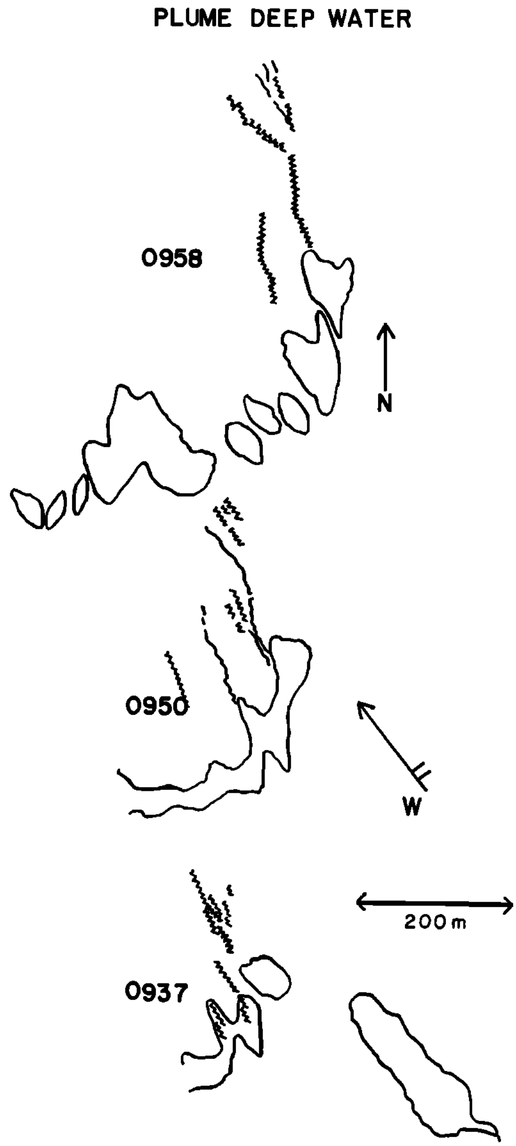

Fig. 5. Tracing of a photographic sequence of a dye stripe over the deep water site (site A). Lines of cards are shown leeward. A patch of the dye pattern from a plume generator is shown in the bottom right corner (March 19, 1970).

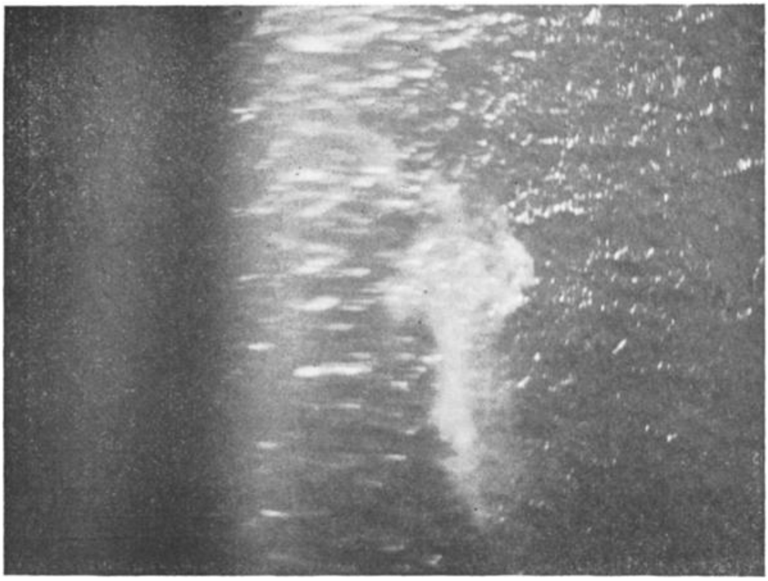

Fig. 6. Photograph of the patch from the plume generator at site A in the morning (0930 hours) March 19, 1970 (see Figure 5).

The Ekman current profile is given by *Ekman* [1905]

$$u = V_0 e^{-\pi z/D} \cos\left(45° - \frac{\pi}{D} z\right)$$
$$v = V_0 e^{-\pi z/D} \sin\left(45° - \frac{\pi}{D} z\right) \tag{1}$$

where $D = \pi(2K/f)^{1/2}$ is Ekman depth or depth of frictional influence, K is eddy viscosity, and f the Coriolis parameter, which in Bermuda is equal to 0.77×10^{-4} sec^{-1}. With the angle between the plumes at 1 and 10-meter depth averaging 30°, we obtain $D = 77$ meters and $K = (D/\pi)^2(f/2) = 225$ cm^2/sec. A similar estimate was independently obtained from the magnitude of the velocity at different depths. The average ratio of the length of the plumes generated at 1-meter depth to that in 10 meters was 1.56 (Figure 10). The plumes at intermediate depths (4 and 7 meters) were regularly distributed between these extremes. Using equation 1, the Ekman depth of 62 meters and the eddy diffusion coefficient of 150 cm^2/sec were derived. It is convincing that similar estimates of eddy viscosity are obtained using both direction and magnitude of the velocity vector.

The estimate of wind stress from the current profile using the Ekman model [*Hunkins*, 1966] is $\tau = \rho V_0 (fK)^{1/2}$. For $K = 150$ cm^2/sec and $V_0 = 10$ cm/sec, $\tau = 1$ dyne/cm^2 compared with an estimate of 0.55 dyne/cm^2 from the wind speed. As there is uncertainty in the wind stress formula (see for example the discussion by *Stommel* [1965]), we can consider that the two estimates are in reasonable agreement. The flow pattern over Plantagenent Bank contained the following 4 elements of the Ekman spiral: (1) deviation of 45° of the surface current to the right of the wind, (2) deviation of the deeper current to the right, (3) decrease of current speed with depth, and (4) reasonable estimate of wind stress.

A qualitative indication of the Ekman spiral in the deep ocean was observed by *Katz et al.* [1965]. A detailed Ekman spiral structure has been measured under the polar ice by *Hunkins* [1965]. However, we believe that the March 19 experiment at site B presents the first Ekman spiral detected in the mixing layer over the open ocean that can be described by constant eddy viscosity.

It is interesting to point out that, in a purely wind-induced shear zone of the Ekman layer, the shear would decrease exponentially with depth. Applying the mixing length hypothesis, the eddy viscosity becomes $K = l^2(\partial\langle u\rangle/\partial z)$. Unless l^2 increases in exactly the same way that

Fig. 7. Photograph of the dye stripe and cards at 0958 on March 19, 1970 (see Figure 5).

$\partial\langle u\rangle/\partial z$ decreases, which is very unlikely, K would be a function of depth. Such a result is contradictory to Ekman's original assumption of constant eddy viscosity. To have constant viscosity with depth, another factor must be involved in the production of the necessary homogeneous turbulence. It is believed that the shallow Plantagenet Bank accomplishes this by destroying the large-scale Langmuir cells. Observation of turbulence created by the bank was reported by *Rossby* [1969].

Thus, the same set-up for detecting an Ekman spiral which 'failed' twice over the deep water was successful over the shallow water. Large plumes deployed by pumping liquid dye from Argus Tower at depths of 6 meters and 1 meter on the same day provide the physical reasoning for this. In contrast to the large stripes over the deep area (Figures 5 and 8), the plumes from the tower (Figure 10) are regular, and no medium or large cells are present. Only small

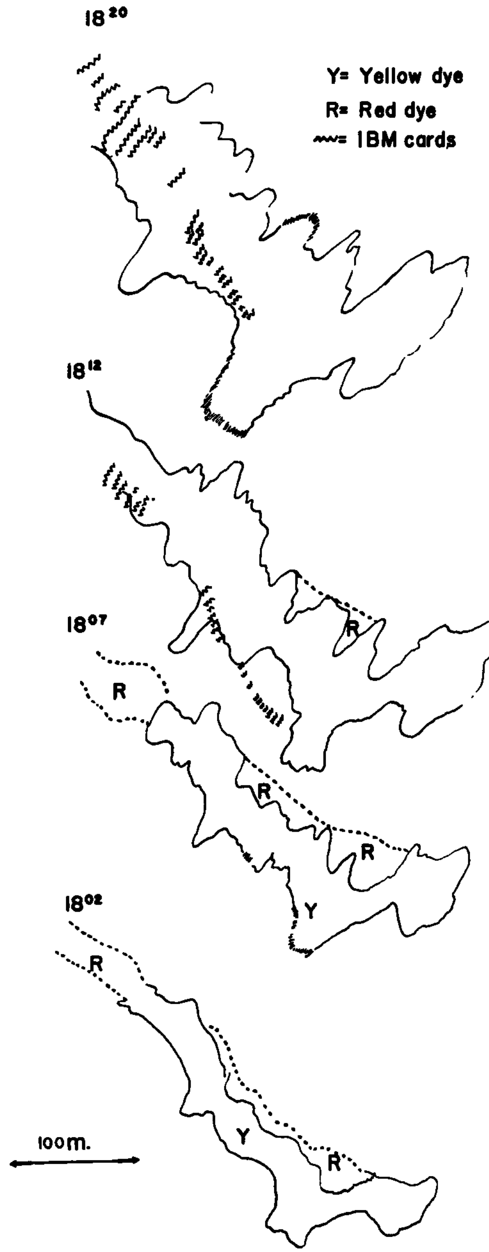

Fig. 8. Tracing of photographic sequence of dye stripe in the afternoon of March 19, 1970.

Langmuir cells (spacing of 4–5 meters) could be detected over the Plantagenet Bank.

Summarizing this experiment, we can say that in a moderate sea with a mixing depth of more than 200 meters we found a complex structure of Langmuir circulation above the deep ocean. These cells are believed to be responsible for the vertical transfer of momentum [*Gordon*, 1970]. The Plantagenet Bank seemed to destroy the large and medium-size Langmuir cells and to transfer their energy into small-size turbulent eddies. In this case, the Ekman spiral

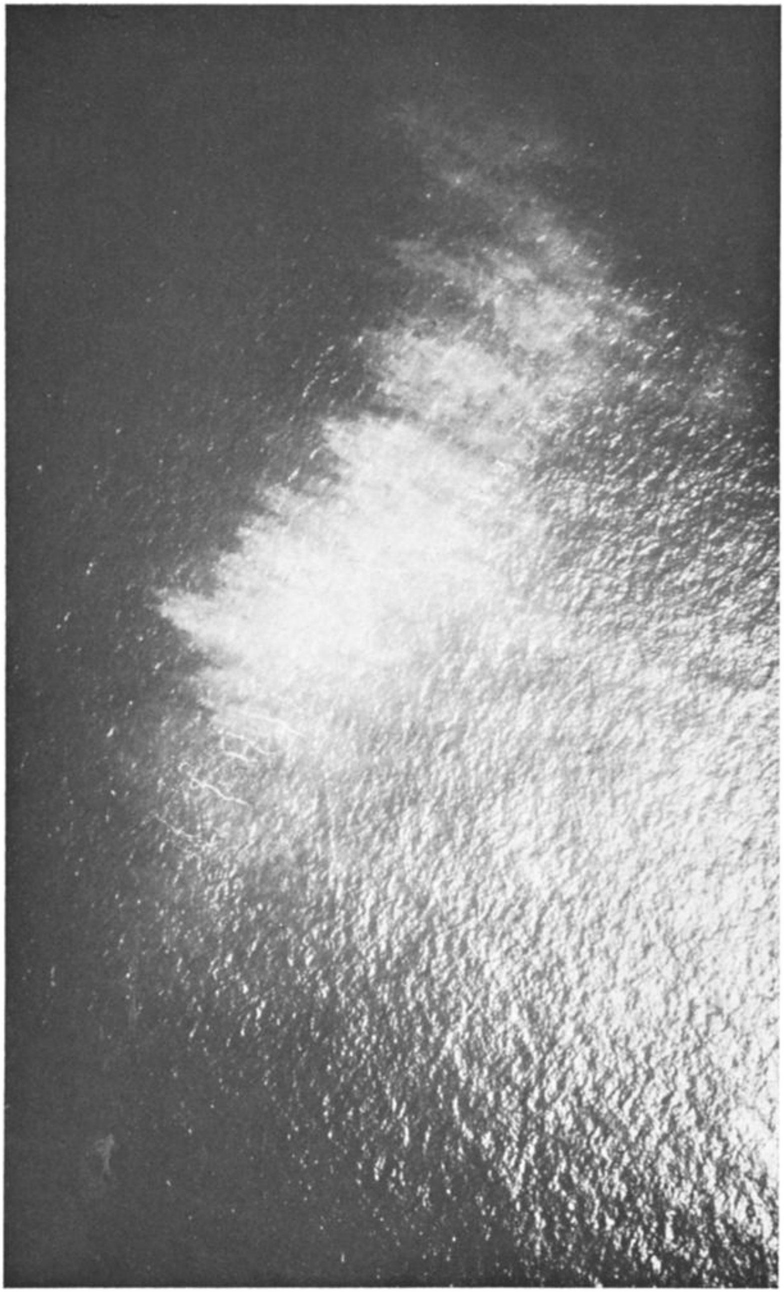

Fig. 9. Photograph of the dye stripe in the afternoon at 1800 hours on March 19, 1970.

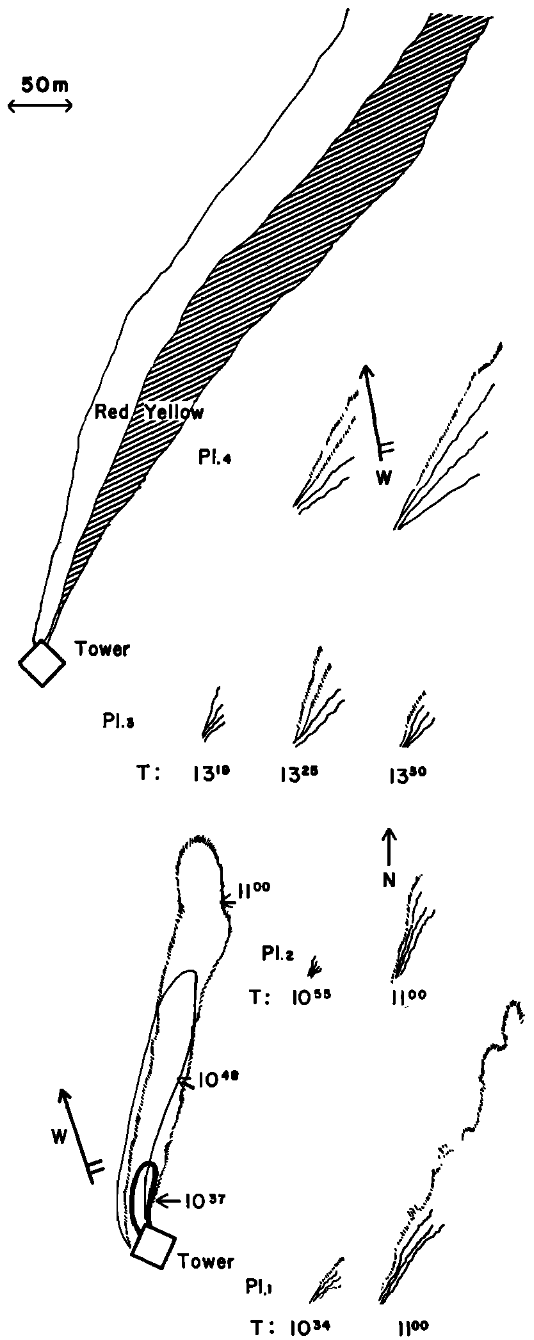

Fig. 10. Tracing of photographic sequence of plumes over site B in the morning (Pl.1, Pl.2) and afternoon (Pl.3, Pl.4) on March 19, 1970 and tracings of the wide plumes from the tower at different times.

is observed and the eddy viscosity is constant with depth.

It should be noted that we found a coexistence between the small-size Langmuir cells and the Ekman spiral. This is probably due to the temporary nature of these small cells.

Experiment of January 29, 1970: Condition with calm wind and net heat transfer to atmosphere. This experiment was carried out over a deep water area south of Bermuda (Figure 3, area A). The meteorological conditions during this experiment, measured at Bermuda, are given in Table 1. The temperature profile was nearly isothermal down to 300 meters, being about 18.3°C, except for the upper meter, which appears on the AXBT trace to have been about 0.6°C cooler.

The experiment was divided into two phases. In phase 1, eight dye bombs were deployed from the aircraft, as described earlier. Figure 11 shows the initial distribution of the dye patches 5 minutes after deployment. At the same time, an anchored multiple dye-plume generator was deployed from a ship nearby. The current in the upper 10-meter depth was found from the plumes to be 30 cm/sec toward the east. Interestingly enough, the four plumes traveled in the same direction. In fact, when photographed from above, a single straight plume to the east could be seen; only in oblique photographs were the other plumes visible.

Another interesting feature of these plumes is their growth rate with distance. In this particular experiment, the width of the plumes grew linearly with time and could be described by a diffusion velocity of 0.2 cm/sec; i.e., $B_{(\mathrm{cm})} = B_0 + 0.2t$, where B is the width of the plume. By comparison, in the March 19 experiment the diffusion velocity of the plumes was about 1 cm/sec. Figure 12 presents the dye field at 0943 superimposed on the distribution at 0929, and one can see the anticyclonic tendency of the dye patches at that period.

Phase 2 of the experiment was started at 1019 hours, 50 min after the first deployment. A set of 9 plastic one-gallon containers of dye was deployed in the vicinity of the first dye patches. The distribution of the dye field at the beginning of phase 2 is given in Figure 13, which also shows continuation of the anticyclonic rotation of the initial dye field. However, the elongation of the dye field shows a cyclonic tendency. The vertical vorticity and horizontal divergence of the dye field were computed for each of these phases (Table 2) by comparing the dye distribution in different periods

$$D = \frac{1}{A}\frac{dA}{dt}$$
$$\zeta = \frac{1}{r}\left(\frac{\partial r^2\dot{\theta}}{\partial r} - \frac{\partial \dot{r}}{\partial \theta}\right) \tag{2}$$

where A is the area enclosed by the centers of the dye patches and r and θ are the polar coordinates. The computation was carried out in areas where it could be seen that the dye patches as a whole were subject to the same motion. The area of the dye patches shrank at a rate that indicated a convergence of 5×10^{-5} sec^{-1}. Figure 14 gives the configuration of the dye field at 1252. The following are the main developments at that period:

1. The dye patches converged into one line, which rotated anticyclonically. However, the dye patches in the line were subjected to cyclonic shear.
2. The new dye patches converged into a parallelogram and were subjected to anticyclonic shear.
3. A strong cyclonic shear prevailed between the line of the old dye patches and the new ones. As a result, the two systems approached each other. This tendency of strong cyclonic shear between the two phases continued until the end of the experiment.

Figures 15 and 16 give the configuration of the dye patches at 1318 and 1335. The area enclosed by the new phase continued to shrink, and the convergence line from phase 1 continued to rotate anticyclonically toward the middle of the new dye patches. In Figure 17 we see the dye distribution at 1417 superimposed on the distribution at the beginning. It should be noted that Table 2 summarizes the vorticity of the dye patches themselves, including the cyclonic shear in the vicinity of the convergence lines. These lines show uniform anticyclonic rotation in the inertial period, i.e., 60° in four hours (Figure 17).

If the two distributions are compared, it can be seen why the concept of turbulent mixing failed to describe the patterns of dye patches in our experiment. The seventeen different dye patches, which at 1019 were in two separate groups, were subject to organized motion which drew them close to each other. The dye patches from the old phase converged into one line, which, at the beginning, was 1 km east of the new dye patches. This line rotated anticyclonically at the inertial rate toward the new dye

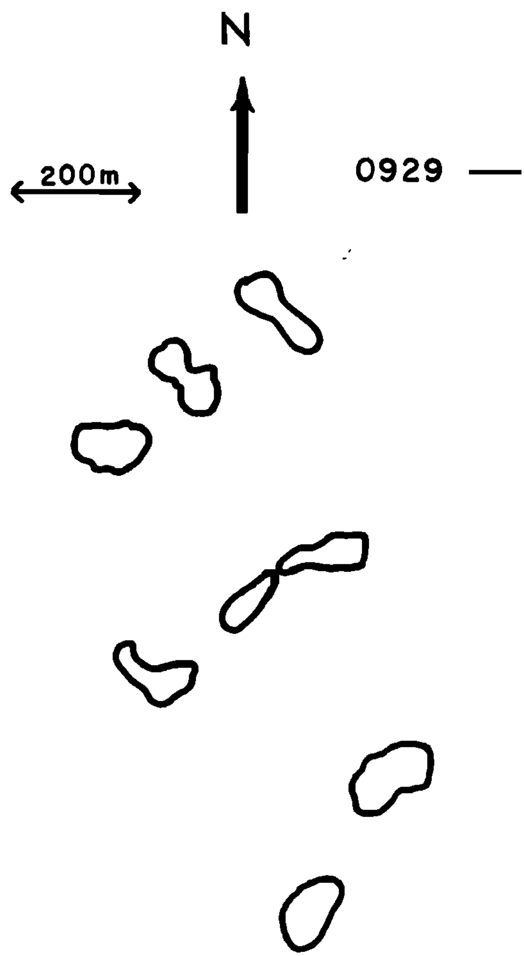

Fig. 11. In Figures 11–17 we have presented the tracings of a photographic sequence showing the development of the dye field in the experiment of January 29, 1970. Each figure presents the dye patches superimposed on the previous distribution (the time sequence is included in the figures). The tracing was done by indexing one dye patch to coincide with the same patch in the previous phase. Thus the mean motion of the dye field is excluded, but the change of orientation is observed. Diamonds indicate lines of *Sargassum*. Figure 11 shows the initial distribution of the dye patches 5 min after deployment of the dye.

Fig. 12. The dye field at 0943 superimposed on the distribution at 0929. The anticyclonic tendency of the dye patches at that period are shown.

patches. The new dye patches also exhibited inertial rotation and at the same time were subjected to convergent flow. This convergent flow started to be very strong at 1250 and toward the end approached 10^{-3} sec^{-1}.

Both the old and the new dye patches started with anticyclonic vorticity and, as they approached the immediate vicinity of the convergence area, the vorticity became cyclonic (Table 2). The angles between the two convergent lines were 100° to 130°. It is interesting to note that the lines of Sargassum weed photographed in this same sequence are parallel to the lines of convergence of the dye patches. At the end of the experiment the Sargassum was trapped along those lines (Figures 14 through 17). Photographs of the dye patches at 1250 (Figure 18) and 1345 (Figure 19) show the above patterns in the later stages of the experiment.

Figure 20 presents the rate at which the variance of the centers of the dye patches relative to the centers of mass changes with time. Apparently the increasing rate is linear with time; and without knowing the process, one could assume that we face a Fickian diffusion. However, the total area covered by the dye field decreased. Thus, the second moment fails to describe the dye pattern of the above experiments. In these experiments the diffusion worked against horizontal convergence, and the mixing was mainly due to small-scale diffusion. Figure 20 also gives the rate of increase of the area of the individual dye patches. The mixing of the dye patches can be characterized by an eddy diffusion parameter of $K = 2200$ cm^2/sec. The mean standard deviation of the dye patches' area during the experiment was one-third of the mean area.

The very dry air and the indication of a small temperature gradient near the surface supports the assumption that the convergent lines are driven by thermohaline instability. The heat budget over the sea surface was calculated

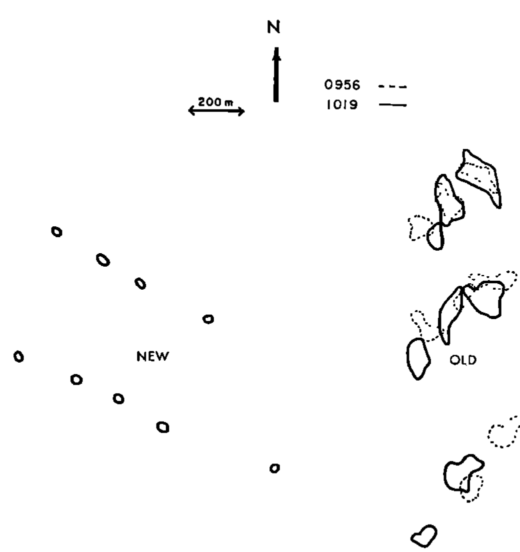

Fig. 13. Distribution of the dye field at the beginning of phase 2. The continuation of the anticyclonic rotation of the initial dye field is also shown.

TABLE 2.

Local Time	A Area, $10^4 m^2$	Time Interval	Divergence A, 10^{-4}/sec	ζ, 10^{-4}/sec
		Old Phase		
0929	10.4	0929–0943	−1.4	−1.4
0935	10.2			
0943	9.2	0943–1019	−0.2	+2.9
0956	9.3			
1019	8.7	0929–1019	−0.55	+1.6
1240	1			
		New Phase		
1019	15.0	1019–1240	−0.66	−2.0
1240	8.4	1240–1252	−1.5	
1252	7.0	1252–1318	−3.3	−8.0
1318	4.1	1318–1335	−4.7	+3.0
1335	2.5	1335–1350	∼−20.0	+3.0
1350	∼0	1019–1335	−1.5	−2.2
		Both Phases		
1019	63.0			
1252	47.0	1019–1252	−0.32	

using meteorological data (Table 1) according to formulas suggested by *Laevastu* [1965]. The results are given in Figure 21, where we see substantial night cooling prior to the experiment.

Other experiments. Table 3 summarizes eleven dye experiments in the Bermuda area (including those already described) and one east of Barbados (in the Bomex working area). The Reynolds number in column 9 of this table is according to the definition of *Faller and*

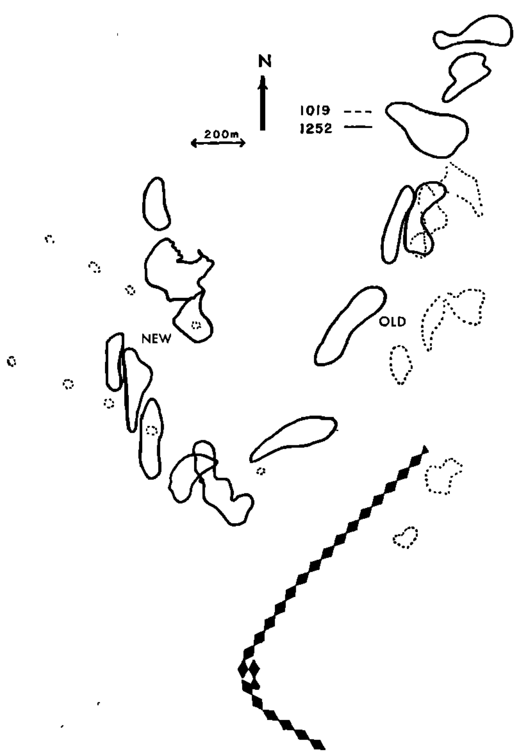

Fig. 14. The configuration of the dye field at 1252.

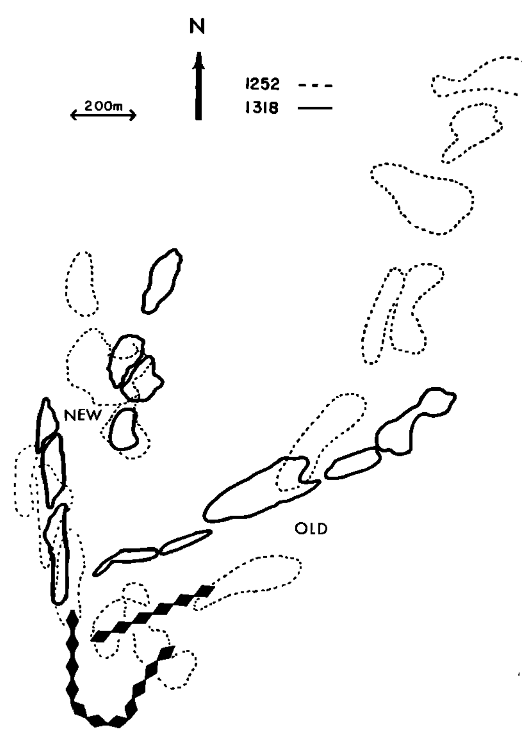

Fig. 15. The configuration of the dye field at 1318.

Kaylor [1966]

$$R_e = \frac{V_0}{(Kf/2)^{1/2}}$$

where surface velocity V_0 was related to the wind speed W by

$$V_0 = 0.02W$$

We also assume that the eddy viscosity of the Ekman flow before transfer into Langmuir circulation is $K = 200$ cm²/sec, as we found over Plantagenet Bank on March 19. This number is speculative, but R_e of 100 seems to be an estimate of the critical condition when Ekman flow becomes unstable. The smallest value under which we obtained large-scale Langmuir cells (March 19) was $R_e = 88$. However, when the depth of the mixing layer was 40 meters (May 7, 1969), large cells were not detected, even when R_e was 120.

When the dye pattern from the plume generators reveal regular plumes with different angles between them, there is a '+' in the Ekman spiral column. This does not mean that the flow followed the Ekman spiral in an exact manner (only on March 19 were the four elements of the Ekman spiral revealed). But the fact that plumes exist can be taken as evidence that the vertical transfer is due to small eddies and their action can be approximated as eddy viscosity.

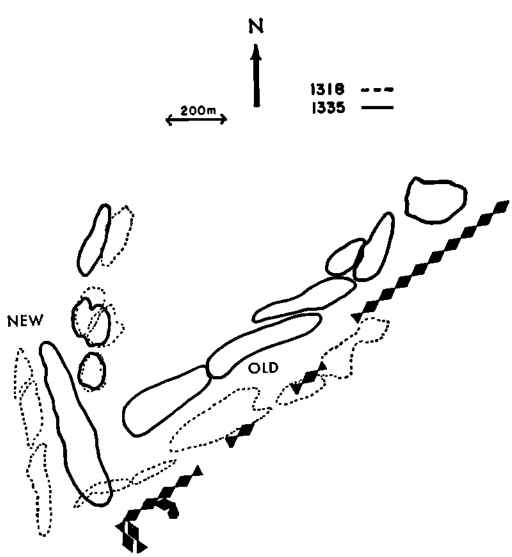

Fig. 16. The configuration of the dye field at 1335.

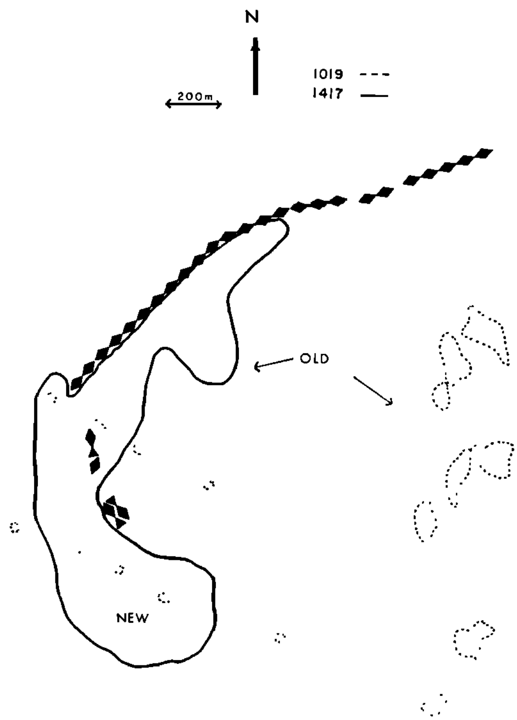

Fig. 17. The dye distribution at 1417 superimposed on the distribution at the beginning.

Summarizing these observations, we can say that, when the wind speed reaches 5 knots, small-size Langmuir cells are developed.

It was suggested by *Langmuir* [1938] and confirmed by *Scott et al.* [1969] that the spacing between the Langmuir cells in Lake George was equivalent to the depth of the mixing layer. However, in the ocean, when the mixing layer is deeper than a few meters, it is observed that the spacing between these cells is not related to the depth of the mixing layer. When the layer is deeper than approximately 100 meters, a surface flow in which only small Langmuir cells are developed is very unstable; and without exception, when the wind exceeds approximately 10 knots, a hierarchy of Langmuir cells is observed. The superimposed scales of 280, 35, and 5 meters already described (March 19) are an example of this hierarchy. Figure 22 (experiment of November 19, 1969) shows a tracing of cells, the largest of which is 90 meters. A hand-held photograph of this dye stripe clearly shows regular cells of 12-meter spacing between the larger cells. At that time the AXBT showed a

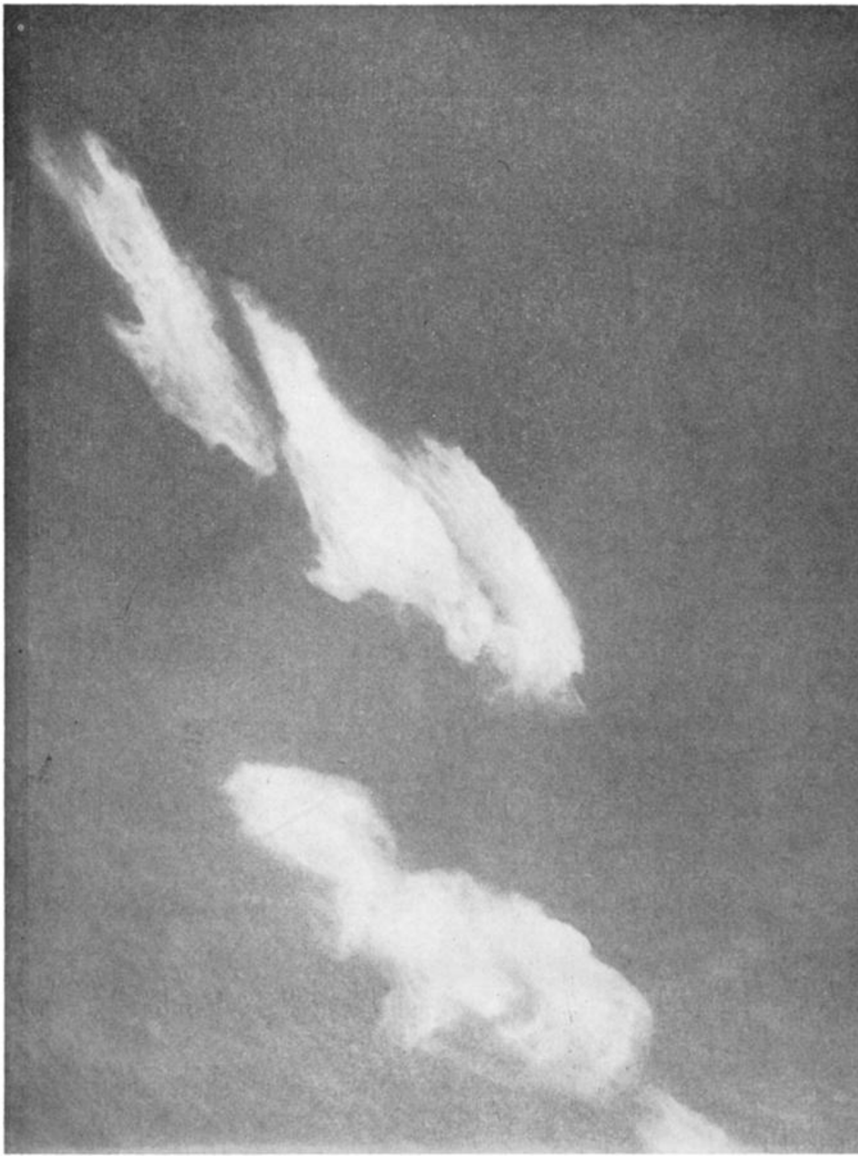

Fig. 18. Photograph of the dye field (new phase) at 1250 January 29, 1970 (see Figure 14).

sharp temperature discontinuity at a 90-meter depth. In the same figure, the dye stripe of August 11, 1969, shows cells of about 30-meter spacing, which was the same as the mixing layer depth at that time (Table 3).

The Plantagenet Bank tends to suppress the development of the largest-scale cells. However, for moderate to strong winds of 15 knots or more, large-scale cells are developed over the bank, and the spacing between the larger cells was 40–50 meters, which is equivalent to the depth of the water over the bank.

Considering all these experiments, we believe that the correlation between horizontal spacing of the larger Langmuir cells and the depth of the mixing layer is well established. It should be mentioned that *Faller and Woodcock* [1964] did not find a correlation between the spacing of the *Sargassum* and the depth of the mixing layer. However, in a later paper *Faller*

[1969] pointed out that the spacing between the *Sargassum* lines was the same, on the average, as the mixing depth.

MAGNITUDE OF FORCES

Experiment of January 29. Calculations of the vorticity associated with the dye fields are given in Table 2. We shall estimate the magnitude of forces by using the vorticity equation

$$\frac{d(\zeta + f)}{dt} = -(\zeta + f)D - (w_x v_z - w_y U_z) + (\alpha_x P_y - \alpha_y P_x) + F_\zeta \qquad (3)$$

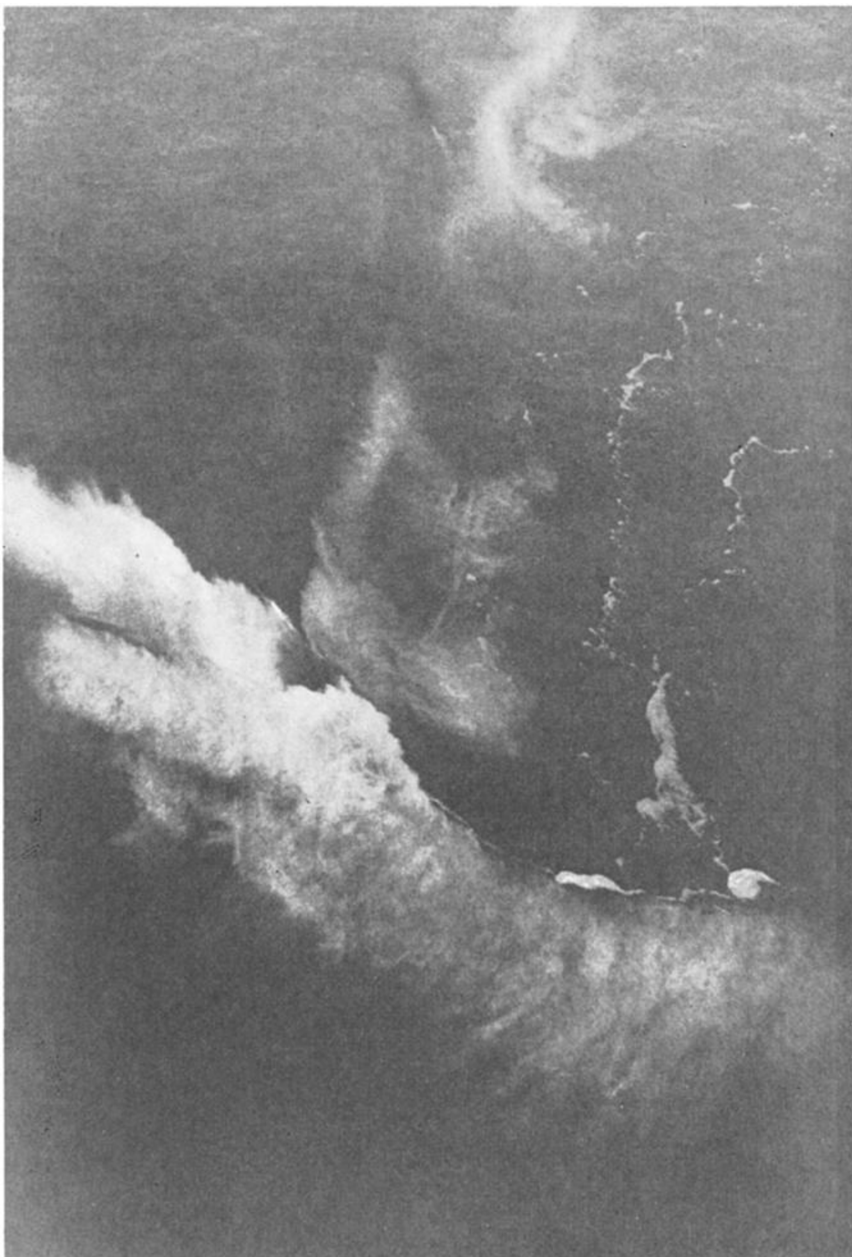

Fig. 19. Photograph of the dye field at 1345 January 29, 1970.

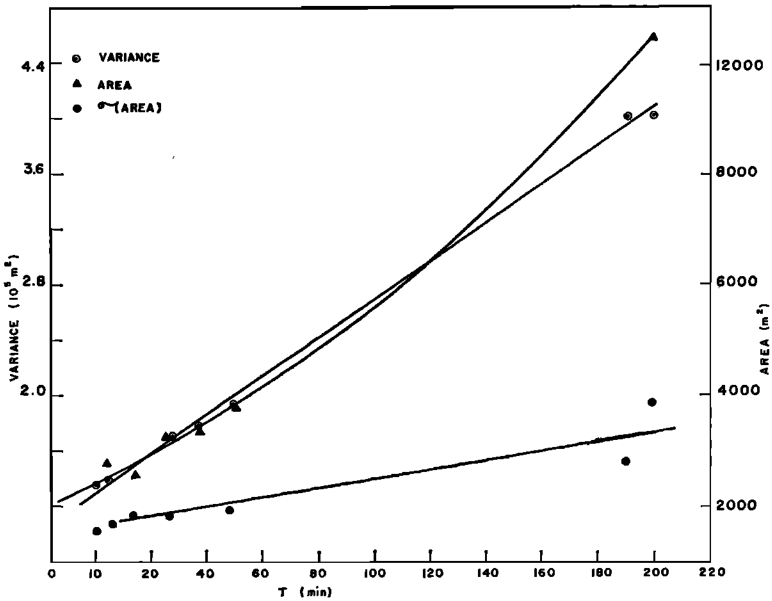

Fig. 20. Graph showing two aspects of the development of the dye field. The total area of dye in different phases of the experiment and its standard error are plotted against time. The variance of the dye patches relative to the center of mass (of the entire field) is plotted against time. In the calculation of the variance each dye patch was treated as a floating point.

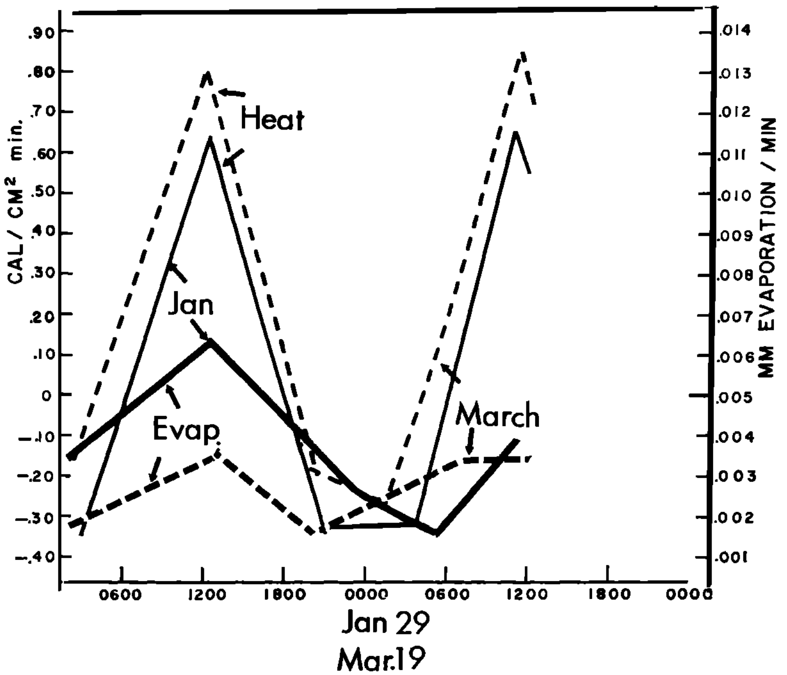

Fig. 21. Heat balance and evaporation, as calculated for March 18–19 and January 28–29, 1970.

TABLE 3. Summary of Experimental Conditions and Results

Date	Area*	Dye Form†	Depth of Mixing Layer, meters	Wind Speed, knots	Mixing Mechanism** Ekman	Small Langmuir	Large Langmuir and Spacing, meters	Turbulent Reynolds No.	Remarks
5/ 1/68	*B*	Bomb patch	50	25	×	+	50	250	Sea state 5–6
5/ 2/68	*B*	Bomb patch	50	20	×	+	44	200	Sea state 4–5
8/21/68	*A*	Stripe, cards	30	10–18	–	+	32	300	Sea state 2–3
3/25/69	*A*	Stripe, cards, anchored plumes	250	6	+	+	–	70	Sea state 1
5/ 7/69	*A*	Bomb patch, stripe, cards	40	12	+	+	–	120	Sea state 2
6/24/69	Barbados	Stripe, cards	10	12	×	+	–		Sea state 2
9/18/69	*A*	Bomb patches, stripe, cards	30	5–8	+	+	–		Sea state 1–2
	B	Anchored plumes, air-drop plumes, metered plume						70	
11/18/69	*B*	Metered plume	50	30	–	+	30–50	300	Sea state 6–7
11/19/69	*A*	Stripe	90	20	–	+	87	200	Sea state 5
1/29/70	*A*	Stripe, bomb patches, anchored plumes	300	0–5	–	+	–	50	Calm–thermal instability
3/19/70	*A*	Bomb patches, stripe, cards, anchored plumes	200	8–9	–	+	280	88	Sea state 2
	B	Air-drop plumes, metered plumes			+	+	–	88	
6/24/70	*A*	Bomb patches		12	–	+	×		Sea state 2–3
	B	Air-drop plumes	7		+	+	×	120	

* Area *A*, deep water site (3000 meters); Area *B*, Plantagenet Bank (50 meters).
** – indicates the given mechanism was not observed; + indicates the given mechanism was observed; × indicates no data.
† See text, 'Experimental Procedures.'

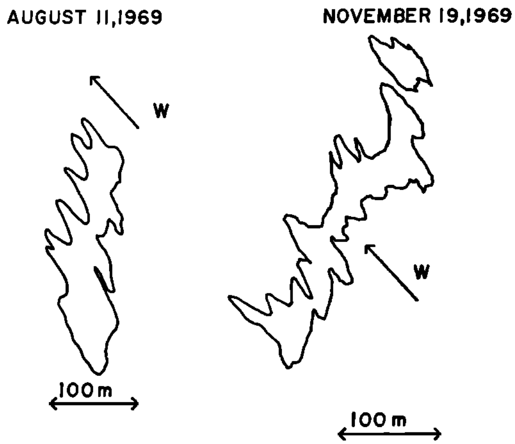

Fig. 22. Tracing of photographs showing dye stripes on November 19 and August 11, 1969 at site A.

where

$$\zeta = \frac{\partial v}{\partial x} - \frac{\partial u}{\partial y}$$

$$D = \frac{\partial u}{\partial x} + \frac{\partial v}{\partial y}$$

α = specific volume

$$F_\zeta = \frac{\partial Fx}{\partial y} - \frac{\partial Fy}{\partial x} = \text{the friction tendency term}$$

Table 2 indicates that the change in the vorticity of the dye patches is from 10^{-7} to 10^{-8} sec^{-2}; i.e., the vorticity of the old phase changed from -10^{-4} to 2.9×10^{-4} within an hour, and the new phase changed from -2×10^{-4} to -8×10^{-4} within three hours. Thus, we can weight the different terms of the vorticity equation accordingly, omitting the terms $df/dt = \beta v = 10^{-12}$. The solenoid term can be important on the convergence line only if it is accompanied by a sharp thermal front. However, the infrared temperature detector (ART) shows variations of less than 1°C (equivalent to 3×10^{-4} variation in density) over the entire area; the size of the eddies was found to be 1 km. The solenoid term, $(fU_g/\alpha)(\partial\alpha/\partial x)$, where Ug is the geostrophic current, can be approximated to be

$$(10^{-4} \times 10)\left(\frac{3 \times 10^{-4}}{10^5}\right) \approx 3 \times 10^{-12}$$

which is four orders of magnitude smaller than the observed variation of the vorticity. As the big cells seem to be curved, we shall write the vorticity equation in cylindrical coordinates (after neglecting the small terms), obtaining

$$\frac{d\zeta}{dt} = -(\zeta + f)D - r\frac{\partial W}{\partial r}\frac{\partial \dot{\theta}}{\partial z} + F_\zeta \tag{4}$$

which assumes that no motion exists at the base of these eddies. The magnitude of the second term can be estimated by assuming that the eddies rotate as a solid disc

$$r\frac{\Delta W}{\Delta r}\frac{\Delta \dot{\theta}}{\Delta z} \approx \frac{W}{H}\dot{\theta} \approx \frac{D\zeta}{2} \tag{5}$$

With these assumptions, the sign of $\partial\dot{\theta}/\partial z$ is the same as ζ, and the sign of $\partial W/\partial r$ is opposite the sign of D. Thus we shall approximate

$$-r\frac{\partial W}{\partial r}\frac{\partial \dot{\theta}}{\partial z} \approx \frac{\zeta D}{2} \tag{6}$$

In principle, the dye patches provide the information on $d\zeta/dt$, ζ and D. With equation 4 F_ζ can be estimated. This might be possible, provided that the dye patches cover an area larger than the eddies and the photographs are taken at close intervals. We plan to do this in future experiments; meanwhile, let us tentatively assume that the friction tends to work against the existing shear, i.e., $F_\zeta = -\kappa\zeta$. Equation 4 becomes

$$\frac{d\zeta}{dt} = -\left(\frac{\zeta}{2} + f\right)D - \kappa\zeta \tag{7}$$

where κ is the non-negative function of space and time. When the vorticity is positive, it can be amplified only when $d\zeta/dt > 0$, or

$$-\left(\frac{\zeta}{2} + f\right)D - \kappa\zeta > 0 \tag{8}$$

which can be written

$$D < -\left(\frac{\kappa\zeta}{\zeta/2 + f}\right)$$

Thus, a cyclonic eddy must be coupled with convergence or decay. This is borne out by our observations, which indicate that the convergence lines were associated with cyclonic shear. When $\zeta < 0$, $|\zeta| = -\zeta$

$$D < \frac{\kappa|\zeta|}{f - |\zeta|/2} \tag{9}$$

For $|\zeta| > 2f, D < 0$; and for $|\zeta| < 2f, D > 0$. Thus an anticyclonic tendency can be amplified in divergent regions, provided $|\zeta| < 2f$ or in convergent regions $|\zeta| > 2f$.

In our experiment the dye patches encountered two different large eddies. Both started with anticyclonic vorticity and ended with cyclonic vorticity. As the dye patches covered part of the eddies, we can only give crude estimates of the divergence and vorticity of these eddies. Certainly the values of $d\zeta/dt$ could be off. Although we cannot determine F_t, the term would appear to be important when the dye patches converge rapidly. We did not observe the anticipated (from equation 7) abrupt change in vorticity in the final phase, which is probably due to the boundary effect in the narrow zone of convergence between two different cells.

Langmuir cells. The only parameter associated with Langmuir circulation that can be determined from the aerial photographs is the forward velocity in the convergence zone. On March 19 this velocity was estimated from the elongation of the dye patches and from the sequential photographs of the dye stripe to be 5–10 cm/sec. At the same time, the wind stress was calculated from the wind speed near the surface. One cannot make a sophisticated model of Langmuir circulation based only on these two parameters. However, reasonable estimates can be made by applying certain basic physical concepts. These can be discussed in relation to the schematic representation in Figure 23.

By following the observations of *Scott et al.* [1969] and our own experience (Figures 6, 7, 8, and 9), we assume that the cell motion is intensified in the convergence zone. Physically, we assume that the heading of the water in the convergence zone is due to longer exposure to the wind stress and that the wind stress penetrates through eddy viscosity into the friction layer, whose depth is Z_f. Thus, the forward acceleration of the water in the surface layer is

$$a = \frac{\tau'}{Z_f} \tag{10}$$

where $\tau' = \tau/\rho$. The time required for such acceleration to produce forward velocity is

$$T = \frac{V_0}{a} = \frac{V_0 Z_f}{\tau'} \tag{11}$$

The characteristic velocity from the upwelling to the downwelling is

$$V = \frac{L/2}{T} = \frac{L\tau'}{2U_0 Z_f} \tag{12}$$

In their review of Langmuir circulation, *Scott et al.* [1969] and *Sutcliffe et al.* [1963] show that four different studies on the downward velocity resulted in linear relations between wind speed and downwelling velocity. This suggests that the forward shear also will increase linearly with wind speed (as the wind stress is proportional to the square of wind speed).

$$U_0 = \frac{\gamma}{2}(\tau')^{1/2} \tag{13}$$

where γ is to be determined from the experiment. By introducing U_0 into equation 12

$$V = \frac{L_a}{\gamma}(\tau')^{1/2} \tag{14}$$

where $L_a = L/Z_f$.

We assume further that, at depth $Z_m = L/2$, the flow is nondivergent and vertical velocity approaches its maximum value. The downwelling and the upwelling at this depth are assumed to

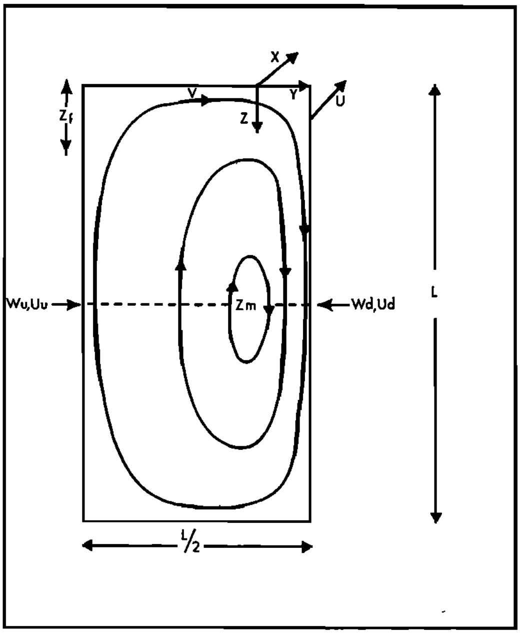

Fig. 23. Schematic of Langmuir circulation.

be sinusoidal.

$$0 \leq y \leq 0.1L \begin{cases} W(Z_m, y) = W_d \sin \dfrac{5\pi}{L} y \\ U(Z_m, y) = U_d \sin \dfrac{5\pi}{L} y \end{cases}$$

$$-0.4L \leq y \leq 0 \begin{cases} W(Z_m, y) = -W_u \sin \dfrac{5\pi}{4L} y \\ U(Z_m, y) = -U_u \sin \dfrac{5\pi}{4L} y \end{cases} \tag{15}$$

As stated earlier, our observations confirmed those of *Scott et al.* [1969] that Langmuir circulation functions as a strong coupling between the surface and deeper part of the mixing layer. Thus we assume that in the Langmuir regime the stress varies very slowly with depth, i.e.,

$$\tau_0' \approx \tau'(Z_m) = \langle UW \rangle$$

The constancy of τ can be justified for $0 < Z < Z_m$, as in this layer W increases with depth due to horizontal convergence and the forward motion U decreases due to internal eddy viscosity. We may assume that these two tendencies will balance the product $\langle UW \rangle$. However, beneath $Z = Z_m$ this product must decrease with depth. By substituting U and W from equation 15 and averaging over y, we obtain

$$\langle UW \rangle = 0.1 W_d U_d + 0.4 W_u U_u \tag{16}$$

From continuity

$$W_u = -W_d/4$$

or

$$\tau'(Z_m) = 0.1 W_d (U_d - U_u) \tag{17}$$

We can assume that the horizontal shear between the upwelling and the downwelling is reduced due to eddy viscosity within the cell. We shall approximate the shear at depth Z_m to be one-half the shear in the near surface, i.e., $U_d - U_u = U_0/2$. Using our observation of $U_0 = 5$ cm/sec and $\tau = 0.5$ dyne/cm^2, the downwelling velocity on March 19, 1970, is approximated to be $W_d = 2$ cm/sec, and the upwelling to be $W_u = 0.5$ cm/sec and $V = 0.4$ cm/sec.

It is interesting to estimate the Langmuir number L_a and γ from equation 13; $\gamma = 2U_0/(\tau')^{1/2} = 14$, and $L_a = (0.4 \times 14)/(\tau')^{1/2} = 8$. For the largest cells ($L = 280$ meters) the expected friction layer would be 35 meters. Similarly, the friction layer for the medium-size cells ($L = 35$ meters) would be 4.5 meters. Thus we may speculate that within the observed hierarchy of cells (5, 35, and 280 meters on March 19, 1970; 12 and 90 meters on November 19, 1969) the friction layer for any size cells is determined by the scale of the next smaller size.

In a study of inertial current oscillation *Pollard and Millard* [1970] found an agreement with observation when they assumed that the wind stress acts as a body force all over the mixing layer. Our observations suggest that the transfer of momentum from smaller to larger cells would be an effective coupling and could explain the rapid response of the mixing layer to the wind stress.

It is of interest to relate the above parameters which characterize the Langmuir circulation to the commonly used vertical eddy viscosity and eddy diffusivity.

Vertical eddy diffusion. We shall equate the flux due to Langmuir circulation with the diffusion flux

$$\langle WC \rangle = -K \frac{\partial \langle C \rangle}{\partial \langle z \rangle} \tag{18}$$

where C is the concentration of soluble matter, the distribution of which is assumed to be uniform and a regular function of depth (i.e., salinity, radon). (The angle brackets denote the mean value over time.) If $\langle C_1 \rangle$ is the mean concentration in the upper layer and $\langle C_2 \rangle$ is that in the bottom layer, we obtain

$$-K \frac{\langle C_2 \rangle - \langle C_1 \rangle}{L/2} = 0.2(W_d C_1 - 4 W_u C_2) \tag{19}$$

By applying our model for sinusoidal distribution of W and by using equation 14 and the relations $W_d = 5V$ we obtain

$$K = 0.32L\, L_a \frac{(\tau')^{1/2}}{\gamma} \simeq 0.18L(\tau')^{1/2} \tag{20}$$

Thus, the vertical eddy diffusivity depends essentially on the size of the cells and wind velocity (since $(\tau)^{1/2} \approx W$). For the medium-size cells on March 19, 1970, $L = 35$, $\tau = 0.5$. We obtain $K = 650$ cm^2/sec. And for the large cells, where $L = 280$ meters, $K = 5300$ cm^2/sec.

The radon method [*Broecker et al.*, 1967] should be useful in estimating the diffusivity associated with Langmuir circulation. Recent radon and dye observations in Lake Ontario in winter by Gerard and Assaf (in preparation) confirmed that the eddy diffusivity associated with Langmuir cells of 100 meters was 1600 cm^2/sec in agreement with our estimate (given above equation 20).

We should emphasize that the validity of the K approximation depends on the regularity of the distribution function, and this in turn depends on the relation between the 'age' of the transport. The criterion for the validity can be written as $T_c < T$, where T_c is the mean life of the Langmuir cells and T the period of the suspended matter in the mixing layer (for detailed analysis, see *Assaf* [1969]). As the momentum flux depends on the correlation of $\langle UW \rangle$, while the diffusion of matter depends only on the vertical motion, we expect that the equivalent eddy viscosity of Langmuir circulation will be different than the eddy diffusivity.

Vertical eddy viscosity. Assuming that wind stress is steady for a period long enough compared with T, we shall write the momentum flux

$$\langle UW \rangle = K_v \frac{\partial \langle U \rangle}{\partial z}$$

$$K_v = -\frac{\tau'}{\partial U/\partial z} = \frac{\tau' \cdot L/2}{(U_1 - U_2)} \qquad (22)$$

where U_1 and U_2 are the mean current in the upper half and lower part of the Langmuir cells, respectively.

SUMMARY

The twelve experiments discussed in this paper reveal three different mechanisms of oceanic mixing: thermohaline, Ekman flow, Langmuir circulation. The thermohaline mixing, characterized by convergence lines of different orientation, was found under calm sea conditions (January 29, 1970). Ekman flow has been observed under moderate conditions (May 7, 25 and September 18, 1969; March 19 and June 24, 1970), but its effectiveness in vertical transport is marginal. The most common and effective mechanism of vertical transport in the mixing layer is Langmuir circulation, and under moderate to strong winds this process dominates the other mechanisms.

Scott et al. [1969] and *Faller* [1969] discussed the following six proposed mechanisms to explain Langmuir circulation: (1) shearing instability, (2) atmospheric vortices, (3) wind-oriented thermal convection, (4) wind profile modification by surface film, (5) radiation pressure on surface film, and (6) wave action. Our observations (Table 3), which indicate that the presence of Langmuir circulation depends on the depth of the mixing layer, as well as on wind stress, tend to rule out numbers 2–6 above as important mechanisms in the formation of medium and large-size Langmuir cells. In particular, the results of our quasi-synoptic experiments at a deep and shallow ocean site (March 19, 1970), having essentially the same wind and sea conditions, support this conclusion. However, the role of wave action (6) in the formation of small Langmuir cells is not in conflict with our observations. Since the vorticity associated with the small Langmuir cells is two orders of magnitude greater than for the larger cells (where the vorticity is equivalent to the earth's rotation), the driving mechanisms may differ.

These results also imply that the deeper the homogeneous layer, the more effective is the mechanical mixing within this layer, as smaller wind stress is required to initiate the larger Langmuir cells. When the mixing layer (or depth) is shallow, light to moderate winds produce only small Langmuir cells (a few meters in size) and mechanical mixing below it will be controlled by relatively ineffective eddy viscosity.

Acknowledgments. We thank Mrs. Alice Mullins for her secretarial duties which included in this case editing of the manuscript. We are grateful to Professor Alan J. Fuller for his helpful comments.

The research reported in this paper was supported by the U. S. Naval Oceanographic Office contract N62306-67-C-0296 and the U. S. Atomic Energy Commission contract AT(31-1)2663.

REFERENCES

Assaf, G., Emanated products as a probe of atmospheric transport, *Tellus, 21,* 820–828, 1969.

Broecker, W. S., Y. H. Li, and J. Cromwell, Radium-226 and radon-222 concentration in Atlantic and Pacific Oceans, *Science, 158,* 1307–1310, 1967.

Ekman, V. W., On the influence of the earth's rotation on ocean currents, *Ark. Mat. Astron.*

Fys., Royal Swedish Academy of Science, 2(11), 1–52, 1905.

Faller, A. J., The generation of Langmuir circulations by the eddy pressure of surface waves, *Limnol. Oceanogr., 14,* 504–513, 1969.

Faller, A. J., and R. E. Kaylor, A numerical study of the instability of the laminar Ekman boundary layer, *J. Atmos. Sci., 23,* 466–480, 1966.

Faller, A. J., and A. H. Woodcock, The spacing of windrows of Sargassum in the ocean, *J. Mar. Res., 22,* 22–29, 1964.

Gordon, A. L., Vertical momentum flux accomplished by Langmuir circulation, *J. Geophys. Res., 75,* 4177–4179, 1970.

Hunkins, K., Ekman drift currents in the Arctic Ocean, *Deep Sea Res., 13,* 607–620, 1966.

Katz, B., R. Gerard, and M. Costin, Response of dye tracers to sea surface conditions, *J. Geophys. Res., 70,* 5505–5513, 1965.

Laevastu, T., Daily heat exchange in the North Pacific, its relations to weather, and its oceanographic consequences, *Comment. Phys. Math., 31*(2), 1–53, 1965.

Langmuir, I., Surface motion of water induced by wind, *Science, 87,* 119–123, 1938.

Okubo, A., Oceanic diffusion diagrams, *Deep Sea Res.,* in press, 1971.

Okubo, A., Oceanic mixing, *The Johns Hopkins Univ. Tech. Rep. 62,* 119 pp., The Johns Hopkins University, Baltimore, Md., 1970.

Pollard, R. T., and R. C. Millard, Jr., Comparison between observed and simulated wind-generated inertial oscillation, *Deep Sea Res., 17,* 813–821, 1970.

Rossby, H. T., A vertical profile of currents near Plantagenet Bank, *Deep Sea Res., 16,* 377–386, 1969.

Scott, J. T., G. E. Myer, R. Stewart, and E. G. Walther, On the mechanism of Langmuir circulations and their role in epilimnion mixing, *Limnol. Oceanogr., 14,* 493–503, 1969.

Stommel, H., Horizontal diffusion due to oceanic turbulence, *J. Mar. Res., 8,* 199–225, 1949.

Stommel, H., The Gulf Stream, 2nd ed., University of California Press, Berkeley, 1965.

Sutcliffe, W. H., Jr., E. R. Baylor, and D. W. Menzel, Sea surface chemistry and Langmuir circulation, *Deep Sea Res., 10,* 233–243, 1963.

(Received February 9, 1971;
revised June 10, 1971.)